

Antenna subsystem solution for Constellation class microspacecraft

Y. Yuriev, V. Angelopoulos, J. H. Primbsch

Space Sciences Laboratory, University of California, Berkeley, CA 94720

K. Hersey, M. Powers

NASA Goddard Space Flight Center, Greenbelt MD 20771

The problem of achieving a high bit rate science data return from a magnetospheric Constellation microspacecraft, in a cost effective, robust way is not trivial. A relatively uniform gain over a large solid angle area is required for launch-and-early orbit operations. A typical approach would be to include more than one antenna. In that case, the distance between antennas is typically a few wavelengths in the S-band range, leading to deep interference nulls in the antenna pattern. In this paper we consider a realistic, self-justified scientific mission, that imposes specific requirements on the RF system. The classical solution to the interference problem is to consider antenna combinations that minimize the nulls and power split and phase lags between the antennas to optimize the pattern. Along those lines we use a commercial electromagnetic simulator for the specific spacecraft geometry considered and achieve an acceptable gain pattern from a two antenna combination. However, for such small spacecraft dimensions considered, diffraction of waves from a single radiator around the microspacecraft may, in some cases, cause a single antenna configuration to outperform a multiple antenna system. We show that rigorously and argue that for certain Constellation class microspacecraft geometries the optimum solution is a single S-band whip antenna.

1. INTRODUCTION

The magnetospheric Constellation mission poses significant challenges for spacecraft design from the point of view of cost, power and weight [Angelopoulos and Spence, 1998]. Constellation spacecraft are required to achieve a factor of 10 reduction in weight and power than typical spacecraft. However, the required transmission rates are not much different than those of traditional spacecraft. Whether data transmission is taking place from perigee, from inbound and outbound legs of an elliptical orbit or from any other part of the orbit, coverage of a large part of the solid sphere is desired. This is because routine attitude control for station-keeping is outside the scope of inexpensive operations. Moreover, if attitude control capability is desired for launch and early orbit operations, inadvertent spacecraft mispointing during spacecraft release or maneuvers can also result in significant link margin losses. Thus, a low-cost, light RF system solution with a relatively uniform antenna pattern is a quest common to all Constellation missions.

The situation is more complex for Constellation microspacecraft whose linear dimension may be a few S-band wavelengths ($\lambda=13$ cm). When multiple antennas are considered to radiate simultaneously, deep interference nulls in the radiation pattern can result from destructive interference, since the distance between the body mounted antennas is a few wavelengths. Moreover, diffraction of the wave power around the spacecraft can be effective at those spacecraft sizes (may depend also on shape). As a result the nulls may extend beyond the directions expected by simple geometrical optics, exacerbating the problem. Experience from past missions indicates that when inadvertent mispointing occurs, such dropouts not only hinder communications but may be disastrous for a mission, because spacecraft commands may be misinterpreted unbeknownst to the operators, further aggravating a problematic situation. Communications at higher frequencies (such as X- or K-band) may alleviate this interference problem. However, aside from being expensive, components in those frequencies are also bulkier because of the use of waveguides, or the increased power dissipation and the use of more involved filters. Both weight and cost considerations could render X- and K- bands

beyond the means of Constellation microspacecraft.

In this paper we chose to address the above issues with a particular mission design in mind. Being specific rather than general allows us to identify clearly the steps that need to be taken towards the final solution and to be explicit regarding the compromises made. The QUATRO mission [Delory et al., 1998, Angelopoulos et al., 1998] whose study we undertook, is composed of four identical spacecraft in highly elliptical (1500 km perigee altitude by ~ 12.5 Re geocentric apogee) orbits. Data which are accumulated throughout the orbit are transmitted over a 12 minute period in the inbound or outbound leg of the orbit. We require a pattern that is isotropic enough but can lead to a sufficient link margin both for engineering data downlink throughout launch and early orbit operations and for science data downlink in the absence of attitude control throughout the year-long mission lifetime.

The RF system for QUATRO and the resultant link margin for ideal spacecraft orientation were discussed briefly in Angelopoulos et al. [1998]. There, an RF solution with two antennas was chosen because it was most evident that in the absence of big interference nulls that combination of antennas would provide a fairly uniform coverage. In this paper we study a single antenna pattern as well and show that for the specific spacecraft structure studied it outperforms a two antenna system and probably all reasonable combinations of multiple antennae for the given spacecraft configuration.

First, we expand on the main elements of the mission, the RF system and the requirements on tracking in Section 2. Based on an orbit study we find the possible spacecraft orientations and the acceptable losses during planned transmission times. In Section 3, we use an electromagnetic simulation software package, to perform an analysis of the antenna EM structure. We initially study a symmetric spacecraft to test solution convergence. Next, we use a realistic spacecraft model to look for asymmetries due to diffraction. Following a parametric study of antenna combinations, power distribution, and phase difference we present a few acceptable solutions. We explain how the three antennas studied (1/4, 1/2 and 3/4 wavelength) result in the interference patterns of the previous section. We argue that a single, 1/4 wave antenna does as good (or better) a job in both null elimination and uniformity as the best case scenario of a two

antenna system and verify that the gain away from the limits of geometric optics is indeed due to diffraction.

2. MISSION REQUIREMENTS

The QUATRO mission spacecraft is built on a simple, robust design and a philosophy of integrating all instrument and spacecraft functions on a single data processing unit (DPU). A magnetometer on a 0.5m-long boom, a plasma ion and electron spectrometer and two energetic ion and electron telescopes are the instruments on board. Data are collected at all times in the orbit and are stored for transmission at the inbound or outbound leg. There is no requirement for data collection during transmission and spacecraft operations. Commanding is minimal and consists of: 1) Instrument and DPU mode-switching for automatic execution during science operations, and 2) Thruster operation sequences for orbit and attitude control during the launch and early orbit phase also for automatic execution.

The maneuvers are classified as either spacecraft reorientations or orbit changes. Reorientations consist of two kinds: 1) Aligning the main thruster along the δV direction of the next orbit change maneuver, and 2) Re-positioning the spacecraft spin plane on the ecliptic plane after a maneuver, i.e. along a direction favorable for solar panel illumination. Reorientations are taking place in “near-real-time” i.e., with operator monitoring of the attitude and position and with an ability to cease the maneuver in case of a deviation away from planned spacecraft attitude and performance as analyzed with a spacecraft simulator model. Modeling of the orbit and attitude data was performed using the Goddard Trajectory Determination System and the Generalized MANeuver program both developed for other NASA missions at GSFC. Additionally, a NASA-developed spacecraft simulator is under modification for inclusion of the fuel motion effects on the attitude and will be the next step-up in modeling.

For a typical apogee-raise maneuver taking place at perigee, the green thick lines in Figure 1 show the location of reorientation maneuver that has to take place to orient the thruster in the δV direction. A similar reorientation takes place during a typical perigee-raise-and-inclination-change maneuver, which takes place near apogee as shown in the same figure. Before and after the apogee burn, thruster reorientations take place at the blue thick lines. During each reorientation maneuver ground-contact is necessary to ensure proper pointing throughout its course. Finally, the science data transmission takes place during the inbound or outbound legs of the final orbit. The red heavy line on the same figure indicates a typical inbound-leg contact for science downlink.

A fixed 200 kbps transmission rate is used for science downlink. From a range of 20000 km the link margin is 5.7 dB using a two-antenna RF system (see Angelopoulos et al. [1998] for details). This link margin is based on a working hypothesis of a 2.7 dBi antenna gain (maximum gain achieved near the spin plane) derived from an early antenna pattern simulation with a relatively isotropic pattern. A fixed 2kbps rate used for engineering downlink allows a 13 dB link margin for communications with the spacecraft at apogee (80,000 km). Uplink margin is a couple of dB smaller, but this factor is not mission-critical because a more powerful transmitter can always be chosen at a small cost increase. In this paper we are concerned with the engineering downlink margin.

Decreasing the spacecraft-ground antenna range increases the link margin. This happens when a contact is scheduled

closer than the maximum allowable range. The spacecraft-to-ground view angle, θ , measured on the spacecraft frame, varies from one contact to another. As this angle changes away from 90° where maximum gain occurs, gain decreases and the total link margin decreases with it.

Figure 2 shows the link margin plotted as a function of time for the orbits of Figure 1, assuming a constant gain versus θ . Time is shown relative to the nearest perigee or apogee, whichever is closer. We can see that the link margin during perigee maneuvers is range-dominated. For L&EO maneuvers this is by design, because those are scheduled to be very close to perigee so as to minimize the time the spacecraft is pointing in an unfavorable orientation for power. For science downlink this is by design: if an antenna can see the spacecraft inside of 20000 km (upper limit) it can typically see it also near perigee. All 12 min long science contacts were selected from much longer contact opportunity intervals to be as close to perigee as possible. This was done to take advantage of the associated range increase; however this does not necessarily lead to the optimum solution, as the effect of the mispointing has not been folded into the choice of the contact segment. The choice of science contacts can be further optimized after the selection of the antenna pattern.

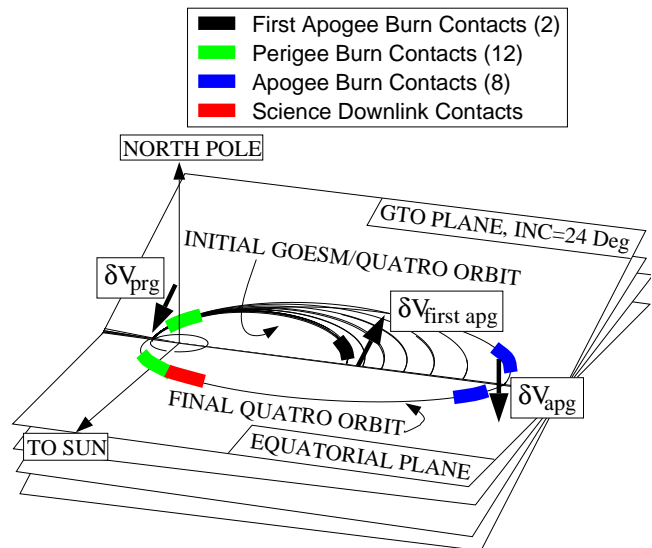


Figure 1. L&EO operations and final orbit in the Geocentric Equatorial Inertial frame. Each orbit-change burn is accompanied by two reorientation maneuvers on either side. Contacts are required during reorientations. Typical locations for these contacts are marked by heavy lines. Typical location for science downlink is marked by a red line.

It is evident from Figure 2 that all perigee L&EO contacts and most science downlink contacts can survive a 15dB drop from imperfect antenna pointing at a typical distance of communication. The apogee maneuvers do not have much gain from range decrease, but because the link margin is 13 dB at apogee, communications can survive an 8dB loss from antenna mispointing that may arise from spacecraft reorientation during those maneuvers. In particular, perigee contacts can withstand even a 30 dB loss from such mispointing.

Figure 3 shows the possible angles θ during L&EO maneuvers and during science downlink. All maneuvers are plotted versus time, centered at the nearest perigee or apogee. Perigee maneuvers have θ values with larger deviations from

90° than apogee maneuvers.

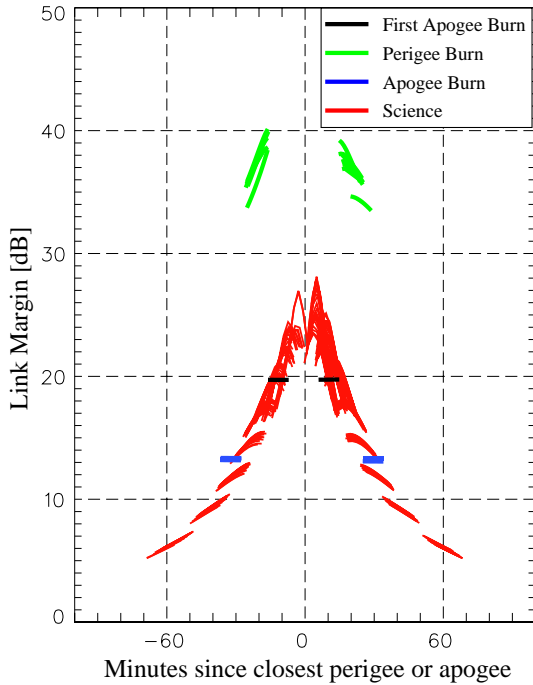


Figure 2. Spacecraft link margin as a function of time since the closest perigee or apogee, assuming a uniform spacecraft antenna pattern. The color scheme of Figure 1 is used to signify the contact type (i.e., red curves are science contacts, blue are L&EO apogee contacts etc.).

Since the perigee contacts are range-dominated, perigee operations can withstand such reorientations more easily than apogee operations where the range decrease is minimal. However, apogee operations are easy for another reason: The fire direction is near the orbit-normal. As a result, the anticipated drop in link-margin during apogee reorientation maneuvers is small, because the reorientations to the fire direction and back to the ecliptic normal do not involve any near-alignment of the spacecraft spin axis (also the wire antenna axis) and the Earth look direction (also the ground station direction). Thus, although at apogee the link margin is antenna-pattern-gain-dominated, the reorientation maneuvers are benign, maintaining good Earth illumination by the spacecraft antenna radiation lobes. Finally, science downlink contacts that cannot withstand a drop more than 15 dB (Figure 2) are precisely the ones further removed from perigee, where the angle θ is near 90°. In summary, maximum deviation of the angle θ from 90° during apogee maneuvers is $\delta\theta_{a,max}=25^\circ$ while during perigee maneuvers and science downlink it is $\delta\theta_{p,max}=\delta\theta_{s,max}=60^\circ$. The above discussion can result in the gain required within a certain angular width for the mission to achieve communications with adequate link margin. This is summarized in Table 1.

The requirements derived from the orbit analysis must also take into account on our ability to maintain spacecraft attitude at the desired orientation. Attitude knowledge within 0.5 degree (three sigma error) or better is possible as derived from an error analysis of the attitude sensor data (courtesy R. Harman). Attitude control is possible to the same level or better by controlling the pulse width of the reorientation thruster to be arbitrarily small. Finally, during science mission phase

the spacecraft attitude remains fixed as no external torques are applied. Thus deviations of the angle θ away from the values derived in the previous discussion can only arise from inadvertent mispointing.

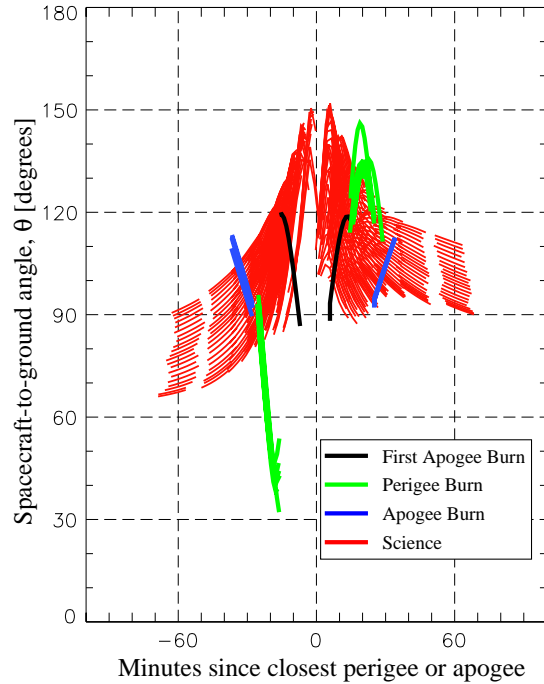


Figure 3. Ground view angles in the spacecraft frame. Elevation angles θ are plotted for all L&EO and science mission contacts, versus time from the closest perigee or apogee.

During L&EO, routine pulse firing of the thruster results in a maximum 2° spin axis change from each pulse. Near-real time operations should take no more than 2 such pulses to verify that the ACS system is performing outside the specification on the basis of comparison with the spacecraft simulator. Adding one more pulse for margin we get a maximum mispointing of 6°. Furthermore, continuous thruster firing causes a helical motion of the spacecraft with a spiral angle required to be 5° maximum. That represents the maximum angle of nutation at the end of the continuous thrusting orbit maneuver. Nutation will damp shortly thereafter, and certainly by the time routine re-acquisition of the spacecraft commences. However, this angle must be added to the total uncertainty, in case immediate acquisition after a fire is required for troubleshooting. This leads to a maximum pointing uncertainty of 11 degrees to be added to $\theta_{p,max}$ and $\theta_{a,max}$. For science phase the uncertainty is equal to the attitude knowledge uncertainty of 0.5 degrees.

In addition to the telemetry requirements discussed above, volume requirements were placed on the spacecraft and those also played a role in the choice of antenna system. The restricted volume arose from the co-manifest opportunity nature of the mission, i.e., by the fact the spacecraft had to fit below the main spacecraft on the launch vehicle, and stay clear of the primary spacecraft and the Centaur stage control electronics and other equipment also mounted on the same payload adaptor. Cost also factored heavily on our system selection, as well as development time. Linear polarization for the spacecraft antenna, and circular polarization for ground transmitter and receiver were selected. This choice was made

despite the 3dB link margin losses due to polarization mismatch because it allows spacecraft communication at any spacecraft orientation, and because by using different handedness in the polarization of the ground receiver and transmitter we achieve inexpensive isolation of the two signals during the planned two-way communications.

The antenna systems that were considered for their simplicity were a wraparound belly-band (coke-can shape), a line (whip) and a combination of whip antennas. The belly-band antenna was dismissed despite its radiation uniformity and low weight, because it had to be mounted at a distance of a few wavelengths from the spacecraft body, along the spin axis. This was forbidden due to volume requirements. A deployable antenna solution was also dismissed so as to eliminate mechanical failure points. Thus, only body-mounted whip antennas were chosen for further study.

	First L&EO Apogee	L&EO Perigee	L&EO Apogee	Science downlink
Typical Excess Link Margin above 5dB	15 dB	30 dB	8 dB	15 dB (most contacts)
Excess Margin Relative to Isotropic	17.7 dBi	32.7 dBi	10.7 dBi	17.7 dBi
Maximum Theta Deviation from 90	30 degrees	60 degrees	25 degrees	60 degrees
Angle Margin	11 degrees	11 degrees	11 degrees	0.5 degrees
Total Angle	41 degrees	71 degrees	36 degrees	60.5 degrees

Table 1. Mission summary of link margin and maximum antenna angles for L&EO and science communications. Excess margin relative to isotropic is the typical excess margin above 5dB plus 2.7 dBi which was used in the computation of Figure 2. Fall-back scenarios for the case of further mispointing are dog-leg maneuvers and automatic sun acquisition.

In our selection of communications frequency we were confronted with a scarcity of choices. We soon realized that the L-band frequency, which would have provided simple, inexpensive and lightweight RF parts, was not available for space communications any longer. NASA scientific missions are now restricted to S-band or higher. Since X-band parts are typically costly and weigh more than their S-band equivalents (because of the aforementioned complexities arising from power dissipation, and filtering) we started considering first S-band communications.

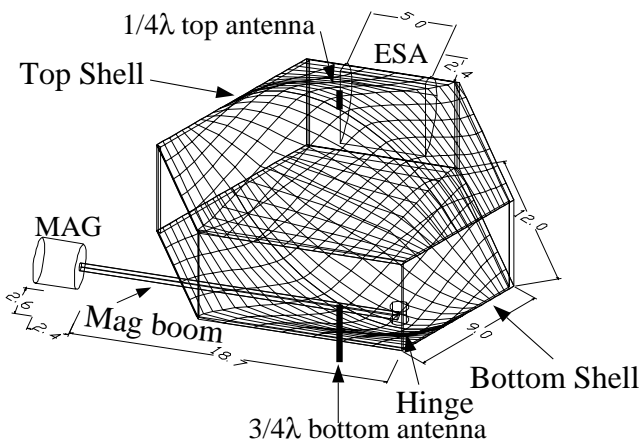


Figure 4. QUATRO spacecraft shape, with magnetometer boom stowed. Dimensions are in inches.

3. ANTENNA SIMULATIONS

Figure 4 shows a three-dimensional outline of the spacecraft which will be spinning about an axis passing from the center of the top and bottom shells. The position of the antenna mountings (along the spin axis) is also shown. The top and bottom shells are covered with metallic foil, which makes them conductive. Thus the body-mounted antennas behave as ground plane antennas. The question we ask is: what is the associated radiation pattern and what is the choice of power and phase fed to the two antennas which optimizes that pattern?

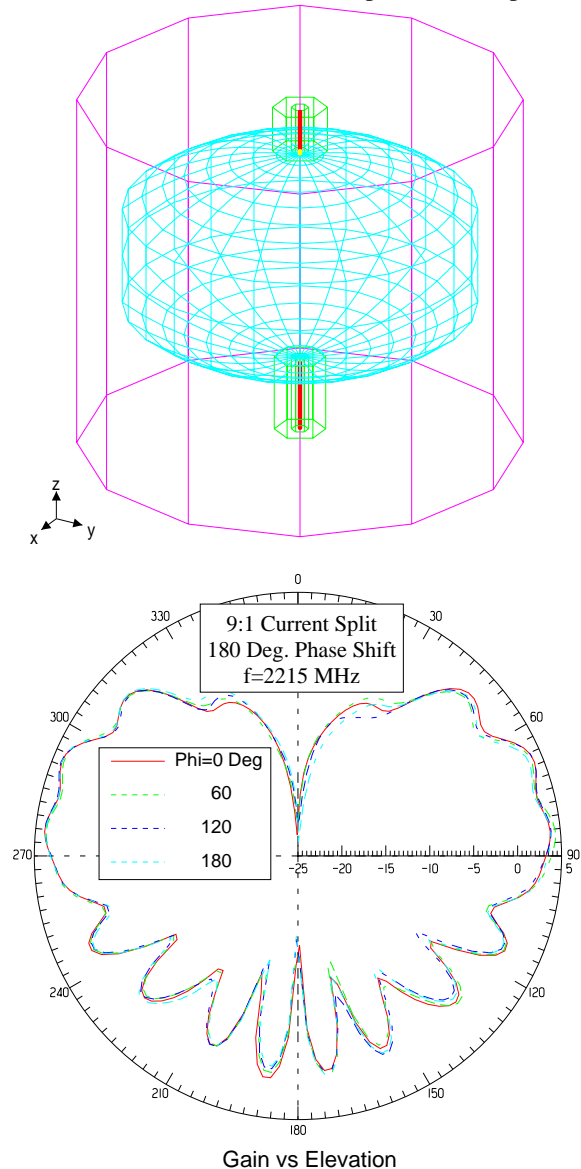


Figure 5. HFSS model and far field optimum solution for a symmetric spacecraft model. The optimum solution results for a 1/4-3/4 antenna combination with a 9:1 current split between the two antennas.

To answer that we used the commercial package High Frequency Structure Simulator (HFSS) by Ansoft. The package simulates currents on surfaces, rather than on wires. It uses finite element methods to compute the field on each surface of a tetrahedron in the free space near the spacecraft. It then propagates the waves away from the source. Consecutive passes improve the solution by increasing the number of tet-

ANTENNA SUBSYSTEM SOLUTION FOR CONSTELLATION MICROSPACECRAFT

rahedra at the locations where the field gradients are maximum. Convergence is proclaimed by the program once two consecutive tetrahedral distributions differ in their results by a specified error or less. This may require an inordinate amount of disk space and computation time. Convergence of the far field patterns may be reached at an earlier stage as evidenced by a set of tests we devised. Those consisted of checking for gain pattern symmetry, and ensuring repeatability of the gain pattern around cylindrically symmetric spacecraft with symmetry implemented slightly differently (e.g., 120 degree symmetry, 15 degree symmetry).

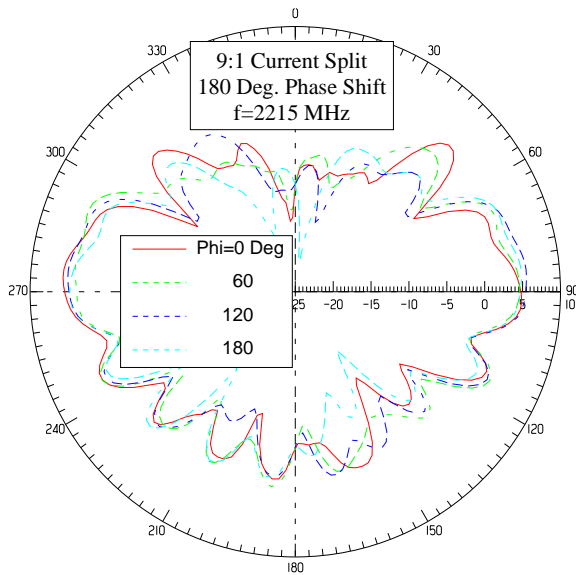
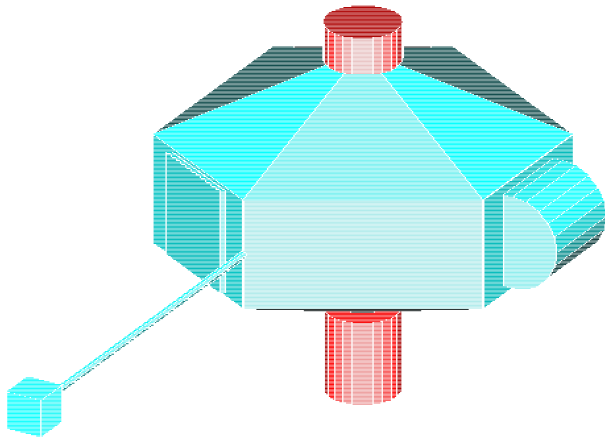


Figure 6. HFSS model and far field optimum solution for a realistic spacecraft model. The optimum solution from the symmetric spacecraft has developed nulls due to interference but remains an acceptable solution.

We then optimized the gain pattern from all possible two-antenna combinations. Figure 5 shows on top the near-cylindrically symmetric spacecraft representation in HFSS. Different antenna sizes were used: 1/4, 1/2 and 3/4 wavelength size. The power split was varied by changing the ratio of currents fed to each antenna and the phase shifts were also varied. The optimum pattern for this antenna configuration resulted from a 1/4 and 3/4 combination of antennas, powered at 180 degrees out of phase with a 9:1 current split. By diverting almost all the power to the top antenna we reduced the interference

with the bottom antenna so that we minimized the nulls, while still keeping a useful amount of power diverted to the 3/4 λ antenna at the bottom hemisphere.

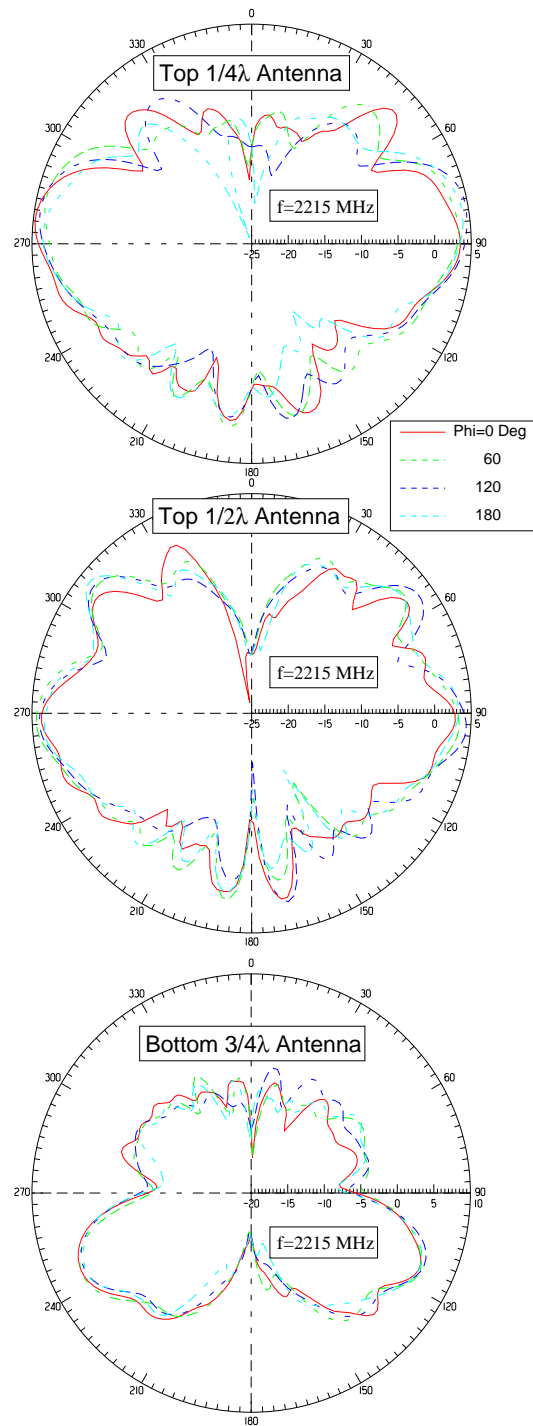


Figure 7. Single antenna pattern solutions mounted on the same spacecraft geometry as in Figure 6.

The next step is to run a more realistic spacecraft model to ensure that the pattern derived from the cylindrical model results in acceptable gain pattern. We show the results from such a run in Figure 6. A similar pattern emerges, only that additional nulls appear partly due to the model used (spacecraft shells are now modeled as planes at an angle) and partly due to the instruments and the deployed magnetometer boom.

Similar arguments explain the lack of cylindrical symmetry. However, the essential features of the gain pattern remain. For $\delta\theta = \pm 41^\circ$ away from 90° no nulls deeper than -10dBi appear, while for $\delta\theta = \pm 71^\circ$ no nulls deeper than -18 dBi are present.

To understand why minimal power diverted to the bottom antenna produces such a good pattern, we also study the individual patterns from each antenna. Figure 7 shows the patterns from a single $1/4\lambda$ antenna (top) and a single $3/4\lambda$ antenna (bottom). A $1/2\lambda$ antenna is shown in the middle for completeness. It is evident that the combined network of antennas of Figure 6 bares close resemblance to the gain of the single $1/4$ antenna. The $3/4\lambda$ antenna inclusion at a finite, although minimal, power results in producing nulls in the directions $\theta = 100$ and 130 degrees.

The original choice of a dual antenna system operating at split power was driven by the desire to move away from a single antenna system that is liable to radiate only within a fraction of a half a solid sphere. However, the above analysis shows unequivocally that a single, $1/4\lambda$ antenna has a uniform enough gain pattern that provides an adequate solution for the mission. We can see that a combination of a $1/4$ and $1/2$ wave antennas will also lead to significant interference nulls, as will a combination of a $1/2\lambda$ and $3/4\lambda$ antenna. At least within the context of this software package, no multiple antenna combination can produce as uniform a pattern as a choice of a single antenna ($1/4\lambda$, $1/2\lambda$, $5/8\lambda$, $1/4\lambda$ ground plane with stubs etc.).

The reason that this was not intuitively obvious is that although diffraction plays an important role in the formation of any single antenna gain pattern for the QUATRO spacecraft dimensions in the frequency selected, this is not typically the case for larger, traditionally built spacecraft.

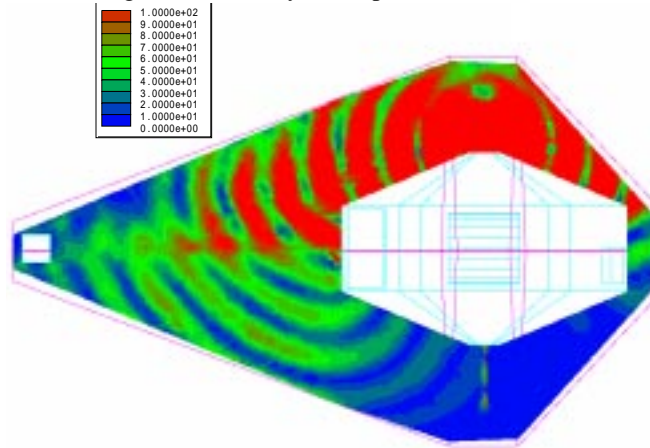


Figure 8. Snapshot from a near-field solution animation for a realistic QUATRO spacecraft. Plotted is the electric field vector magnitude. Consecutive frames show the propagation to be around, as opposed to away from, the spacecraft.

To reassure ourselves that diffraction is indeed responsible for the ability of a single, body mounted antenna to radiate outside the boundaries imposed by geometric optics, we produced an animation of the electric field magnitude distribution around the spacecraft (near field of view). The alternative explanation that we wanted to dispel was that the off-geometric-limits radiation might be due to induced spacecraft surface currents, which reradiated. That situation is difficult to simulate, as it depends on a very accurate representation of

the surface material properties and is affected by coatings and spacecraft handling prior to launch. Conversely, diffraction only depends on spacecraft size, shape and wavelength.

Figure 8 shows a snapshot of the wave propagation animation. Consecutive time frames show that at angles $\theta = 120$ degrees or greater the propagation of the wave is around the spacecraft, not away from it, as would have been the case for surface current radiation. Standing waves are set up at the bottom antenna because the antenna acts as a resonant object. There is no radiation moving away from the bottom antenna. By repeating the simulation in the absence of the bottom antenna the same radiation pattern emerges, i.e., the bottom antenna does not cause re-radiation of power at large θ angles. Another way of expressing this is that the Poynting flux has a zero normal component to the spacecraft body underneath the top shell. We have also plotted the Poynting flux to verify the above scenario. Additionally the surface currents on the bottom shell were zero to within the numerical errors of the simulation. Finally, the same antenna pattern results from running the simulation after introducing a gap (free space) between the top and bottom segments of the spacecraft.

4. CONCLUSIONS AND DISCUSSION

In the selection of an RF solution for Constellation microspacecraft, simplicity is an important consideration that influences all other aspects of the problem: schedule, cost, robustness and fault tolerance. In this paper we started with a realistic mission that has many elements common to proposed Constellation microspacecraft. By being a self-justified mission with well focused objectives, QUATRO poses very clear requirements on telemetry which must be met by a low cost, but robust RF system. By using a state-of-the-art electromagnetic simulator and a realistic spacecraft model we have produced solutions on the gain pattern that are compatible with launch and early orbit as well as routine science data transmission requirements. In doing so we had to run a thorough parameter search because given our spacecraft geometry a multiple antenna system in the S-band range suffers from interference nulls for a large portion of the parameter space considered. This limitation turns out to be the strength of RF systems in support of microspacecraft missions: Interference is aided by signal diffraction around the spacecraft body, which is comparable in size to the RF wavelength. Since radiation diffraction is sufficient to create interference nulls from multiple antennas it must be that a single antenna must produce sufficient gain at large angles to the line-of-sight direction. This has been shown rigorously using the electromagnetic simulator by plotting the single antenna gain and has been confirmed by animating the radiation propagation and computing the Poynting flux.

For the microspacecraft size, shape and wavelength chosen, a single $1/4$ antenna is sufficient for RF communications during all mission phases and superior to all two antenna combinations studied. With one antenna there is no need for a diplexer, a hybrid and an additional cable. This minimizes signal losses that would have arisen from the added components as well as from power division. The gain introduced from avoiding the combined antenna system is ~ 1 dB (0.3 dB from hybrid, 0.5 dB from power reduction, 0.3 dB from cable losses on one additional cable). This gain was included in the original link margin analysis and should be removed if a single antenna is used. Additional benefits over a two antenna system are spacecraft weight and volume reduction, cost re-

duction and robustness. Overall system simplification significant although its direct effects are harder to quantify.

As a final verification of the ability of a $1/4\lambda$ body-mounted antenna to provide sufficient link margin during all mission phases we plotted in Figure 9 that link margin as a function of time. The figure is constructed by taking into account the $1/4\lambda$ gain pattern from Figure 7 subject to the time series of angles θ from Figure 3 and the range-dependence from Figure 2. It includes the added 1dB benefit from a simpler, single antenna. It shows that indeed a very small number of possible science contacts fall below the comfortable limit of 5dB link margin. The margin can be optimized by selecting for downlink the 12 minute interval within the contact opportunity period that has the highest link margin (rather than selecting the 12 minute interval of smallest range, as was done in Figure 9). It can also be further optimized by choosing the spacecraft spin axis direction to be a few degrees off the ecliptic normal in order to optimize the ground station view angles, without affecting much the thermal or power design of the spacecraft. These considerations are beyond the scope of this paper.

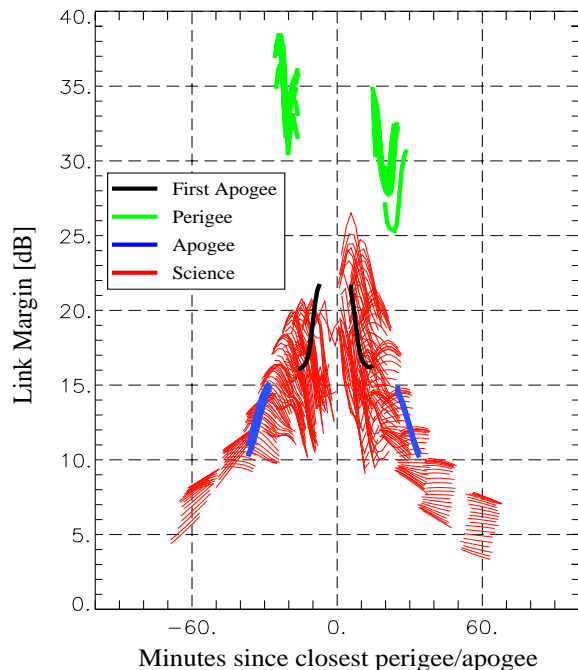


Figure 9. Realistic link margin as a function of time for the entire mission, using a single $1/4\lambda$ body mounted antenna (for antenna pattern shown on top of Figure 7).

While the specific solution studied in this paper was derived specifically for the QUATRO mission, both the procedure we developed for mission analysis, and the lessons learned in the process are applicable to Constellation microspacecraft. It is noteworthy that decreasing the communication frequency to the L-band can result in a number of benefits: First, in the L-band wavelength, diffraction around microspacecraft is even more pronounced. As a result, the gain will become a smoother function of elevation while protruding instruments will have an even smaller effect on the azimuthal symmetry of the radiation pattern. This will result in a much more robust configuration, that relaxes attitude control requirements from the main spacecraft. Second, RF components in the L-band range are less expensive than those in the S-band range by a factor of 10.

Third, ground antennas in the L-band do not require solid surface and are, again, much less expensive than solid surface dishes. This opens up the possibility of building a small number of large, identical, automated Constellation-specific ground antennas around the world. The monetary benefits from circumventing the DSN and the existing large solid surface antennas are obvious. Currently, NASA has withdrawn from the L-band range, leaving it to commercial and military satellites. However, it is possible that special agreements can be made for the purposes of Constellation, a matter requires further investigation.

Acknowledgments. We are grateful for the contributions of the GSFC/GNCC office, in particular R. DeFazio, P. Gates, R. Harman and J. Toth. Contributions of UC Berkeley students M. Somoza, J. Xie in porting the GSFC software packages to UCB, R. Milan in the initial efforts of time-dependent link margin modeling, and G. Y. Lee in spacecraft 3-dimensional modeling are gratefully acknowledged. We wish to thank the Ansoft Corporation for providing us with an educational licence of the HFSS software. This work was supported by CALSPACE grant CS-55-97 and by NASA grant NAGW-5019.

9. REFERENCES

- Angelopoulos, V., and H. Spence, Magnetospheric constellation: Past, present, and future, in *The Physics of Sun-Earth Plasma and Field Processes*, AGU monograph series, Ed. by J. L. Burch, 1998.
- Angelopoulos, V., et al., Tracking and operations of constellation microspacecraft, in *Science closure and enabling technologies for constellation class missions*, UC Press, (this volume) 1998.
- Delory, G. T., et al., A high science return, low-cost Constellation pathfinder, in *Science closure and enabling technologies for constellation class missions*, UC Press, (this volume) 1998.
- V. Angelopoulos, J. H. Primbsch, and Y. Yuriev, Space Sciences Laboratory, University of California, Berkeley, CA 94720-7450, USA (E-mail: gdelory@ssl.berkeley.edu)
- K. Hersey and M. Powers, NASA Goddard Space Flight Center, Greenbelt MD 20771, USA (E-mail: Ken.Hersey@gssc.nasa.gov)

